Beyond ray tracing for internal waves. I. Small-amplitude anelastic waves

Joshua T. Nault and Bruce R. Sutherland[a]
Departments of Physics and of Earth and Atmospheric Sciences, University of Alberta,
238 CEB, Edmonton, Alberta T6G 2G7, Canada

We compute the transmission of small-amplitude two-dimensional anelastic internal waves in nonrotating inviscid fluid having arbitrarily specified stratification and background velocity. Whereas stability analyses of the flow involve solving an eigenvalue problem that relates the frequency to horizontal wavenumber, we focus upon the evolution of waves incident from below with independently specified frequency and horizontal wavenumber. A numerical method is developed to ensure that the wave field in the upper domain corresponds only to upward-propagating transmitted waves. Two particular applications are discussed. First, internal waves incident upon a piecewise-linear shear layer are examined and their transmission is computed as a function of the bulk Richardson number Ri_b and the ratio of the density scale height relative to the depth of the shear layer. The waves transmit partially across critical levels if they coincide with heights where the gradient Richardson number is less than 1/4. Transmission is larger if Ri_b is smaller. Decreasing the density scale height reduces the frequency and wavenumber range over which internal waves propagate, but this does not significantly affect the magnitude of transmission. Second, internal waves generated by flow over Jan Mayen island are examined. Although the waves are ducted, the waves are found to transmit partially through the top of the duct. The results are used to interpret the discrepancy between predictions of the Fourier-ray tracing model and fully nonlinear numerical simulations of Eckermann *et al.* [Mon. Weather Rev. **134**, 2830 (2006)]. © 2008 American Institute of Physics. [DOI: 10.1063/1.2993167]

I. INTRODUCTION

Due to the restoring forces of buoyancy, internal gravity waves (or more briefly, "internal waves") propagate through air having increasing potential temperature with height, $\bar{\theta}(z)$. Internal waves vertically transport energy in such stably stratified fluids leading to drag and mixing at levels where they break. As such, they significantly affect the general circulation of the atmosphere.[1,2] Because smaller spatial-scale waves are unresolved by general circulation models, they necessarily must parametrize their influence. Heuristically applying linear theory and, in particular, ray theory,[3,4] typical parametrization schemes in part assume that the waves break above levels where anelastic growth leads to overturning unless at lower altitudes they encounter a critical level, where their horizontal phase speed matches the background flow speed. Furthermore, they assume that the waves reflect from a level where their Doppler-shifted frequency matches the background buoyancy frequency. Above such a level the waves are evanescent. However, if the depth over which the waves are evanescent is finite, the waves may partially transmit across the region. Although the phenomenon certainly occurs in the atmosphere, such dynamics are not accounted for by a heuristic application of ray theory unless care is taken to match oscillatory solutions to Airy functions near the reflection levels.[5]

For example, internal waves generated by a storm near Darwin, Australia have been observed in the ionosphere.[6,7] Examination of the background wind and stratification showed that the waves were evanescent through part of the mesosphere, but were nonetheless able to transmit partially across this region.[8,9]

Likewise, partial transmission across an evanescent layer of mountain-generated waves has been observed in the lee of Jan Mayen Island, which is situated in the North Atlantic. Using atmospheric profiles taken on the same day as the Jan Mayen experiment,[10,11] Fourier-ray tracing models and fully nonlinear numerical simulations were run in an attempt to capture the dynamics of the waves. They showed that the waves were ducted, being trapped in the troposphere by a level in the lower stratosphere above which the waves were evanescent over a small vertical distance. However, the ray tracing model results differed from the numerical simulation, the latter showing significant wave propagation well into the stratosphere.

The purpose of this study is to provide a computationally efficient means with which to predict the transmission and reflection of internal waves through arbitrary background states and so assess energy transport in the atmosphere. For example, the flow over Jan Mayen took hours for a fully nonlinear model and minutes for the ray theory model to compute.[10] The calculation we perform produces results in seconds, thus making this approach more amenable to operational forecasting.

The transfer of energy between two ducts has been studied by Eckart[12] and Fritts and Yuan,[13] but they focused upon resonant modes that had vertical wavelengths comparable

---

[a]Author to whom correspondence should be addressed. Electronic mail: bruce.sutherland@ualberta.ca.

with the vertical extent of the ducts. The energy transfer was not unidirectional but oscillated between states in which energy was concentrated primarily within one duct and the other.

Analytic formulae have been derived for the one-way transfer of energy by waves crossing a stationary, weakly stratified region,[14] by hydrostatic waves crossing a nonuniformly stratified shear layer,[15–19] and by nonhydrostatic waves crossing a piecewise-linear shear layer.[20] The last showed that the appropriate measure of the transmission coefficient for waves in shear is the ratio of transmitted to incident pseudoenergy flux, a measure proportional to the flux of wave activity. Unlike energy, this quantity is conserved for waves in a background shear flow.

To predict transmission coefficients for waves propagating in arbitrary background states, Nault and Sutherland[21] developed a numerical code that integrated the Taylor–Goldstein equation. Typically, this equation is used to examine stratified shear instability (e.g., see Drazin and Reid[22]), which involves the solution of an eigenvalue problem. For example, to determine the temporal stability of a parallel flow, the complex frequency is determined as a function of the real-valued horizontal wavenumber. The corresponding eigenfunction determines the structure and energetics driving the instability.

The transmission of waves through a parallel flow is fundamentally different from a stability calculation. It is not an eigenvalue problem, but rather one of determining the amplitude of waves at the top of the domain as a function of the amplitude of the incident waves at the bottom of the domain. In such a problem, the frequency and horizontal wavenumber of the incident waves are independent of each other. They are set by the generation process (e.g., by flow over topography or by convective storms) and do not depend on the stability properties of the stratified flow through which the waves consequently propagate.

The usual form of the Taylor–Goldstein equation is restricted to the Boussinesq approximation, which is well suited to internal waves that propagate over distances much smaller than a density scale height. However, non-Boussinesq (i.e., anelastic) effects cannot be neglected when considering transmission across evanescent layers of comparable depth to the density scale height.

Anelastic extensions to the Taylor–Goldstein equation[23–25] have been used to determine the stability of stratified shear flows,[26] but the transmission of incident internal waves through an arbitrarily specified background flow, stable or otherwise, has yet to be studied.

The results presented here extend the study of Boussinesq internal wave propagation[21] to the propagation of anelastic internal waves. The work includes nonhydrostatic effects and is not limited to the Wentzel–Kramers–Brillouin (WKB) approximation of ray theory. This study is restricted to two dimensions, and so does not account for the effect of veering winds.[27,28] The study is also restricted to the examination of small-amplitude waves, although weakly nonlinear effects associated with moderately large amplitude waves are considered in a companion paper.[29]

Section II presents the theoretical background and nu-

merical methods used to compute internal wave transmission in an anelastic gas. In Sec. III the numerical methods are applied to a piecewise-linear shear layer and the results are compared to analytic predictions made in the Boussinesq limit.[20] Section IV examines internal wave propagation observed in the lee of Jan Mayen Island. A summary of the significant findings is given in Sec. V.

II. THEORY AND NUMERICS

The anelastic approximation assumes that the background potential temperature varies slowly in the vertical.[30,31] By considering only the background density in the continuity equation, the fastest time scale upon which fluid motions occur is set by internal gravity waves.[32] Thus, like the Boussinesq approximation, the anelastic approximation filters vertically propagating sound waves. However, the anelastic approximation also accounts for a significant background density decrease in the vertical. This changes the dynamics of internal waves in that their amplitude must increase as they propagate upward in order to conserve momentum.

The fully nonlinear equations of motion in the anelastic approximation are[31,33,34]

$$\frac{\partial \boldsymbol{u}}{\partial t} + (\boldsymbol{u} \cdot \nabla)\boldsymbol{u} = -\nabla(c_p \bar{\theta} \tilde{\pi}) - c_p \bar{\pi}' \tilde{\theta} \hat{z},$$

$$\frac{\partial \tilde{\theta}}{\partial t} + (\boldsymbol{u} \cdot \nabla)\tilde{\theta} = -w \bar{\theta}', \tag{1}$$

$$\nabla \cdot (\bar{\rho} \boldsymbol{u}) = 0,$$

in which primes denote ordinary z-derivatives. Here c_p is the specific heat at constant pressure. The total velocity field is denoted by $\boldsymbol{u}$. The density, $\rho \equiv \bar{\rho}(z) + \tilde{\rho}$, potential temperature, $\theta \equiv \bar{\theta}(z) + \tilde{\theta}$, and Exner pressure, $\pi \equiv \bar{\pi}(z) + \tilde{\pi}$, have been decomposed into background and perturbation components.

The total Exner pressure is given explicitly in terms of the pressure p by

$$\pi = \left(\frac{p}{p_{00}}\right)^\kappa, \tag{2}$$

where p_{00} is the ground level pressure and $\kappa \approx 2/7$ for dry air. The potential temperature is given in terms of the Exner pressure by

$$\theta = \frac{T}{\pi} \tag{3}$$

for air at temperature T. The background Exner pressure and potential temperature are related through background hydrostatic balance by

$$\bar{\theta}\frac{d\bar{\pi}}{dz} = -\frac{g}{c_p}. \tag{4}$$

As in the derivation of the Boussinesq Taylor–Goldstein equation, it is assumed that disturbances are small amplitude, two dimensional, and that the velocity field may be decom-

posed into a steady horizontal background flow superimposed with the perturbation velocity due to waves,

$$\boldsymbol{u} = [\bar{U}(z) + \tilde{u}(x,z,t), 0, \tilde{w}(x,z,t)]. \tag{5}$$

The fully nonlinear equations (1) may thus be written as a single partial differential equation in terms of the mass flux streamfunction $\psi(x,z)$ defined implicitly by

$$(\tilde{u}, \tilde{w}) = \left(-\frac{1}{\bar{\rho}}\frac{\partial \psi}{\partial z}, \frac{1}{\bar{\rho}}\frac{\partial \psi}{\partial x} \right). \tag{6}$$

The resulting equations may be Fourier decomposed in time and horizontal space which amounts to examining solutions for disturbances with extrinsic (ground-based) frequency ω and horizontal wavenumber k. That is, we assume ψ can be written as

$$\psi(x,z,t) = \phi(z)e^{i(kx-\omega t)}, \tag{7}$$

in which $\phi(z)$ is the amplitude envelope of the mass streamfunction, and it is understood that the actual structure of the waves is given by the real part of ψ.

The result of these manipulations gives the anelastic version of the Taylor–Goldstein equation,[24]

$$\phi'' + \frac{1}{H_\rho}\phi' + k^2 \left(\frac{N^2}{\bar{\Omega}^2} + \frac{\bar{U}''}{k\bar{\Omega}} + \frac{\bar{U}'}{k\bar{\Omega}H_\rho} - 1 \right)\phi = 0, \tag{8}$$

in which the intrinsic (Doppler-shifted) frequency is

$$\bar{\Omega}(z) \equiv \omega - k\bar{U}(z), \tag{9}$$

the squared buoyancy frequency is

$$N^2 \equiv \frac{g}{\bar{\theta}}\frac{d\bar{\theta}}{dz}, \tag{10}$$

in which g is the acceleration of gravity, and the density scale height is

$$H_\rho \equiv -\bar{\rho}\left(\frac{d\bar{\rho}}{dz} \right)^{-1}. \tag{11}$$

Equation (8) is more general than that originally defined by Scorer[35] in that is does not assume the waves have zero phase speed or, equivalently, zero intrinsic frequency ($\Omega=0$). By keeping the fourth term in the coefficient of ϕ, we allow for nonhydrostatic effects and thus generally account for the dynamics of waves that have intrinsic frequency close to the local buoyancy frequency N somewhere in the flow.

In the Boussinesq limit, $H_\rho \rightarrow \infty$ for all z, in which case Eq. (8) reduces to the usual Boussinesq form of the Taylor–Goldstein equation, as expected. Anelastic effects are included through the two terms involving H_ρ. Whereas most studies[35–37] further manipulate the equation through the transformation $\phi = \Phi \exp(z/2H_\rho)$, we do not do this, so retaining the $(1/H_\rho)\phi'$ term.

$N(z)$ and $H_\rho(z)$ are not independent quantities but are related by the thermodynamic relationship between the background potential temperature and density. Formulae relating them are given in Appendix A.

The dispersion relation for anelastic waves in uniform background flow, $\bar{U}(z)=U_0$, and in uniform stratification, $N=N_0$, is determined immediately from solutions of this equation. The vertical structure is represented by

$$\phi(z) = e^{z/2H_\rho}e^{\pm imz}, \tag{12}$$

where the vertical wavenumber m is defined implicitly by the well-known dispersion relation for anelastic internal waves,

$$\Omega = N_0 k / \sqrt{k^2 + m^2 + \frac{1}{4H_\rho^2}}. \tag{13}$$

The effects of compressibility are manifest through the finite value of H_ρ in Eqs. (12) and (13). As the background density decreases with height, the amplitude of the waves must grow in order to ensure that the flux of momentum remains constant. Compressibility effects also change the dispersion relation of internal waves. At fixed wavenumber vector, the frequency decreases in media with smaller H_ρ. In particular, whereas Boussinesq waves are evanescent (meaning $m^2 < 0$) if their frequency exceeds the buoyancy frequency N_0, the frequency at which anelastic waves become evanescent is smaller than N_0. Explicitly, evanescence occurs if $\Omega > \Omega_r$, where

$$\Omega_r = N_0 / \sqrt{1 + 1/(2H_\rho k)^2}. \tag{14}$$

More generally, with explicitly specified upper and lower boundary conditions, Eq. (8) can be integrated iteratively to determine eigenfunction solutions corresponding to eigenvalues $\omega \equiv \omega(k)$. This has been done in the anelastic approximation for unbounded shear and jet flows and for shear flows in the presence of a free-slip horizontal lower boundary.[26]

In this study we assume waves are incident from below and may partially transmit and reflect within the domain. The reflected waves propagate downward through the bottom of the domain without influencing the incident waves, for example, by reflecting off a solid lower boundary: the lower boundary condition is not explicitly specified. Thus the problem is not one of finding eigensolutions that represent vertical modes of the domain having frequency a function of horizontal wavenumber. We have the freedom to specify the frequency and horizontal wavenumber independently, but the solution for ϕ is restricted by the causality condition that requires waves at the top of the domain to propagate upward, not downward.

A. Numerical solution method

Given profiles of N^2 and $\bar{U}$, we wish to calculate the transmission coefficient for waves incident from below that have prescribed horizontal wavenumber k and extrinsic frequency ω at the bottom of the domain. After arbitrarily specifying a lower boundary condition for ϕ and ϕ', it is straightforward to integrate Eq. (8) and so determine the structure of the disturbance everywhere in the domain and, in particular, at the top of the domain.

The Heun method[38] is used to integrate Eq. (8), except near singular points, where the coefficient of the ϕ term be-

comes large as a consequence of Ω becoming small. This is where internal waves encounter a critical level. Here we restrict ourselves to examining circumstances in which waves do not encounter a critical level or in which the waves encounter a critical level where the gradient Richardson number Ri_g is less than $1/4$. In the latter case it is straightforward to step over the singularity using an approximate analytic solution provided by applying the method of Frobenius, as discussed in Appendix B.

The transmission of Boussinesq internal waves across a uniformly stratified hyperbolic tangent shear layer was examined by Van Duin and Kelder.[18] More generally transmission across a critical level with $\mathrm{Ri}_g > 1/4$ was examined by Booker and Bretherton.[39] They applied the Frobenius method by extending the frequency to the complex plane and thus showed that the amplitudes of both the transmitted and reflected waves change through linear interactions with the mean flow. Meanwhile the vertical wavelength decreases to zero at the critical level (see Appendix B), implying that large amplitude and viscous effects, neglected by their theory, must also play an important role in determining the nature of wave transmission across a critical layers.[40,41] Such dynamics are beyond the scope of this work and so we do not calculate the transmission coefficient for waves traversing a critical layer where $\mathrm{Ri}_g > 1/4$. If $0 \leq \mathrm{Ri}_g < 1/4$, the vertical wavelength is nonzero at the critical level and so the consideration of large amplitude and viscous effects is less important.

The challenge in determining the characteristics of propagating waves in nonuniform media comes through establishing the appropriate lower boundary condition for ϕ and ϕ'. The amplitude and phase of the waves at that boundary are the superposition of an incident, upward-propagating wave, and a reflected downward-propagating wave. An arbitrary lower boundary condition will result in a disturbance at the upper boundary which is also a superposition of upward and downward-propagating waves. The goal is to choose the lower boundary condition appropriately so that the disturbance at the upper boundary corresponds only to upward-propagating waves. By causality, such waves exist as a consequence of the transmission of the incident waves upward through the domain.

The correct choice of lower boundary condition is done by taking two incorrect guesses for the (complex) wave amplitude at the lower boundary and then superimposing them so that the disturbance at the upper boundary corresponds to an upward-propagating wave alone.[21] Explicitly, incident and reflected wave amplitudes A_1^+ and A_1^- are arbitrarily selected and the corresponding outgoing and returning wave amplitudes at the top of the domain, B_1^+ and B_1^-, are calculated after integrating the anelastic Taylor–Goldstein equation (8). Next different arbitrary amplitudes A_2^+ and A_2^- are selected, and the corresponding outgoing and returning wave amplitudes B_2^+ and B_2^- are found. Finally, by superimposing the first two solutions, correct amplitudes A^+ and A^- are calculated such that $B^- = 0$. Thus the resulting integration of the Taylor–Goldstein equation gives a disturbance with outgoing amplitude B^+ and no returning amplitude at the top of the domain.

The calculation is performed only for values of ω and k

specified so that the incident wave at the bottom of the domain and the transmitted wave at the top of the domain are indeed propagating and not evanescent. This may be established in advance by ensuring $\Omega \leq \Omega_r$ at either vertical extreme of the domain. For anelastic waves with $\|kH_\rho\| \ll 1$, the condition $\Omega < \Omega_r$ highly restricts the range of frequency and wavenumber combinations that permit wavelike solutions at the upper and lower boundaries.

For ω and k corresponding to propagating wave solutions at the boundaries of the domain, the numerical solution produces the profiles of $\phi(z)$ and, in particular, the amplitudes A^+ and A^-, respectively, of the incident and reflected waves at the bottom of the domain and the amplitude B^+ of the transmitted wave at the top of the domain.

The reflection and transmission coefficients are defined, respectively, as

$$\mathcal{R} = \frac{|A^-|^2}{|A^+|^2} \quad \text{and} \quad \mathcal{T} = 1 - \mathcal{R}. \tag{15}$$

$\mathcal{T}$ corresponds to the ratio of transmitted to incident pseudoenergy flux.[20] In the absence of background shear, its value is the same as the ratio of transmitted to incident energy.

III. PIECEWISE-LINEAR SHEAR

As a test of the methods discussed in the previous section, the code is applied to the piecewise-linear shear profiles considered in the Boussinesq approximation by Brown and Sutherland.[20] The profiles are extended to include anelastic effects associated with a finite density scale height. Explicitly, the background flow and squared buoyancy frequency profiles are given by

$$\bar{U}(z) = \begin{cases} U_0 & \text{for } z \geq 2L \\ \dfrac{U_0}{L}(z - L) & \text{for } L \leq z \leq 2L \\ 0 & \text{for } z \leq L \end{cases} \tag{16}$$

and

$$N^2(z) = \begin{cases} N_0^2 & \text{for } z > 2L \\ 0 & \text{for } L \leq z \leq 2L \\ N_0^2 & \text{for } z < L, \end{cases} \tag{17}$$

respectively. The N^2 profile and corresponding plots of potential temperature are shown in Fig. 1.

The strength of the maximum shear relative to the maximum buoyancy frequency is described by the bulk Richardson number $\mathrm{Ri}_b = (N_0 L / U_0)^2$.

Exploiting the piecewise-linear structure of the profiles, analytic formulas for the transmission coefficient of Boussinesq waves can be found[14,20] as a function of ω, k, and Ri_b. This is plotted for $\mathrm{Ri}_b = 100$, 10, and 1 in the first row of Fig. 2. In these plots, the incident wave frequency has been nondimensionalized by the background buoyancy frequency at $z = 0$ so that $\hat{\omega} = \omega / N_0$, and the horizontal wavenumber has been nondimensionalized by the gap width so that $\hat{k} = kL$.
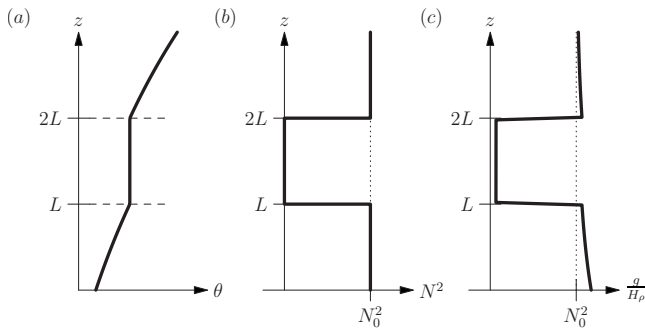
FIG. 1. Profiles of (a) background potential temperature, (b) squared buoyancy frequency, and (c) g/H_ρ, the density based squared buoyancy frequency, plotted for $H/L=1$.

Only results with positive frequencies are plotted. The transmission coefficients for waves with negative frequencies can be determined by symmetry,

$$\mathcal{T}(-\omega, k) = \mathcal{T}(\omega, -k). \tag{18}$$

In the anelastic approximation, the density scale height can vary with z, even where N is constant. Given the definition of N^2 in Eq. (17) and using the formulas in Appendix A, we compute $H_\rho(z)$. For conceptual convenience this is plotted in Fig. 1(c) as g/H_ρ, which represents the squared buoyancy frequency based on the background density.

We define H to be the density scale height at the bottom of the domain and so characterize the importance of anelastic effects in terms of the ratio H/L. Using the profiles prescribed by Eqs. (16) and (17), transmission coefficients are found for $\mathrm{Ri}_b=100$, 10, and 1 and for $H/L=100$, 10, and 1. These are plotted in the bottom three rows of Fig. 2. In each of the plots the superimposed broken white lines highlight special boundaries in $\hat{\omega}-\hat{k}$ space. The dashed lines denote the boundary between regions where solutions are wavelike and not wavelike at the top of the domain for the equivalent Boussinesq system (i.e., where $\Omega|_{z=3L} = \pm N|_{z=3L}$). The dashed-dotted lines mark the boundary between regions where waves do and do not encounter a critical layer somewhere in the flow (i.e., where $\Omega|_{z=3L}=0$).

The second row of plots in Fig. 2, for which $H/L=100$, provides a diagnostic test on the numerical solver. Because the density scale height is two orders of magnitude larger than the barrier depth, anelastic effects are expected to be insignificant. Indeed, comparing these plots to the corresponding analytic Boussinesq results above, we find no quantitative difference between the results, as anticipated.

The transmission of Boussinesq internal waves across a stratified shear layer[20] is briefly reviewed here. In the limit $\mathrm{Ri}_b \to \infty$, the background flow is zero. In this case, for waves at fixed horizontal wavenumber maximum transmission occurs for incident waves with frequency $\omega = 2^{-1/2}N_0$. As Ri_b decreases from 100 (the left column of plots) to 10 (the middle column) to 1 (the right column), the strength of the shear increases. In part, this limits the range of $\hat{\omega}$ and $\hat{k}$ for which the Doppler-shifted waves at the top of the domain are propagating. In the strong shear case, $\mathrm{Ri}_b=1$, the parameter space of $(\hat{k}, \hat{\omega})$ subdivides into two parallelogram-shaped re-
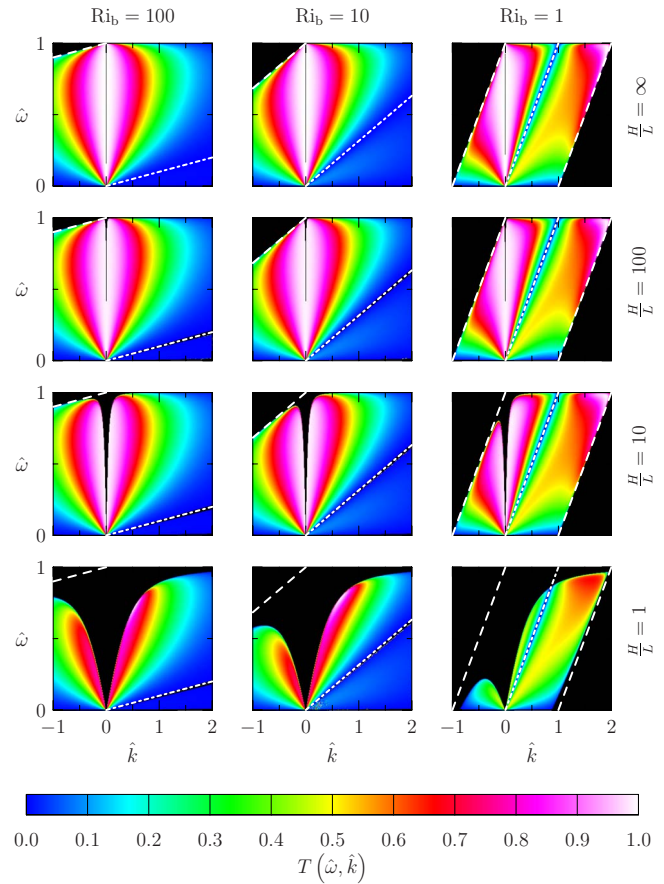

FIG. 2. (Color online) Transmission coefficient $\mathcal{T}$ plotted as a function of nondimensional incident wave frequency, $\hat{\omega}=\omega/N_0$, and wavenumber, $\hat{k}=kL$, for waves incident upon a nonuniformly stratified piecewise-linear shear flow. The bulk Richardson number is constant for each vertical column and the relative density scale height H/L is constant for each horizontal row, as indicated. The Boussinesq predictions ($H/L=\infty$) are computed from an analytic formula (Ref. 20) and plots with finite H/L are computed using the numerical solver. The black regions denote values of $\hat{\omega}$ and $\hat{k}$ for which the Doppler-shifted waves are evanescent at the top of the domain and, hence, for which zero transmission occurs.

gions. The rightmost region corresponds to values of $\hat{k}$ and $\hat{\omega}$ for which incident waves encounter a critical level as they pass through the shear layer. Note that the choice of background profiles being examined here requires that $\mathrm{Ri}_g=0$ where waves encounter a critical level and so our criteria for applying the Frobenius method is always satisfied. As in previous studies,[39,18] we find that waves do indeed transmit across critical levels with $\mathcal{T}$ being close to unity in the case with $\mathrm{Ri}_b=1$ when $\hat{\omega} \simeq 1$ and $\hat{k} \simeq 1$.

Now we examine the influence of anelastic effects which become significant as the ratio H/L becomes small. As H/L decreases from 100 to 10 (the third row of plots) and 1 (the bottom row of plots), the obvious influence is the decreasing range of parameter space $(\hat{k}, \hat{\omega})$ for which the transmission coefficient can be calculated. This is because the critical value of Doppler-shifted frequency Ω_r at which the waves are evanescent at the top of the domain decreases as Hk decreases. The value of Ω_r at the top of the domain is also a function of the bulk Richardson number Ri_b. As Ri_b decreases the Doppler-shifted frequency decreases for
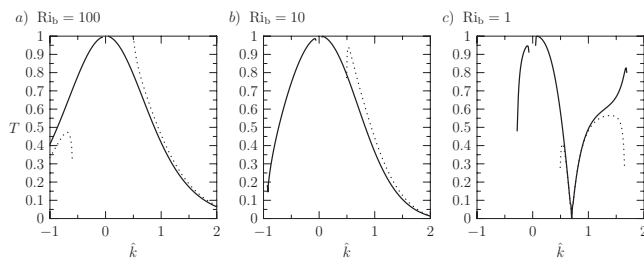
FIG. 3. Transmission coefficients for waves with $\hat{\omega}=0.7$ computed in piecewise-linear shear flows with (a) $Ri_b=100$, (b) $Ri_b=10$, and (c) $Ri_b=1$. Plots are shown for cases with $H/L=10$ (solid lines) and $H/L=1$ (dotted lines).
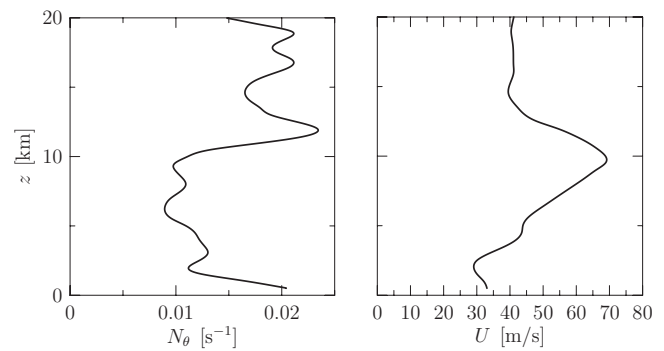

FIG. 4. Buoyancy frequency and mean horizontal wind observed over Jan Mayen at 1200 UTC on 25 January 2000. [Adapted from Eckermann *et al.* (Ref. 11).]

rightward-propagating waves ($\hat{k}>0$) and increases for leftward-propagating waves ($\hat{k}<0$).

More subtle is the relative change as a function of H/L of the transmission coefficient in regions of parameter space where $\mathcal{T}$ can be computed. Although illustrated by the color contours in Fig. 2, for clarity we also include Fig. 3, which plots the transmission coefficient as a function of $\hat{k}$ keeping $\hat{\omega}$ fixed at 0.7. This value of $\hat{\omega}$ is chosen because it corresponds approximately to the frequency of waves that have peak transmission through an N^2-barrier with no shear.[14] The curves are computed for three values of Ri_b and each panel plots the transmission coefficient for the moderate and strong anelastic cases, $H/L=10$ and 1, respectively.

For all three values of Ri_b, we find little difference between the transmission coefficient computed with $H/L=10$ and the corresponding Boussinesq result (not shown). Only near regions of parameter space where $\Omega \lesssim \Omega_r$ do we find anelastic effects slightly reduce the value of $\mathcal{T}$. This is evident by the change in slope of the solid curves near $\hat{k}=0$.

Anelastic effects become more pronounced in the case with $H/L=1$ (indicated by the dotted lines in Fig. 3). In regions of parameter space where the coefficient can be computed, we find the coefficient decreases if $\hat{k}<0$. If $\hat{k}>0$ the transmission increases in cases of weak shear, but it decreases in the case with $Ri_b=1$.

In all circumstances, the change in transmission coefficient from the Boussinesq case is largest in regions of parameter space where $\Omega \lesssim \Omega_r$ for waves not encountering a critical level. Examining the contours in the rightmost parallelogram region of the right column of plots in Fig. 2, it is evident that anelastic effects reduce transmission most strongly for waves crossing a critical level if they are nonhydrostatic, $0.5 \lesssim \hat{\omega} \leq 1$.

IV. WAVES ABOVE JAN MAYEN ISLAND

Jan Mayen Island, located at $(71°N, 8.4°W)$, is an ideal candidate for internal wave generation and propagation studies due to its relative isolation in the North Atlantic Ocean and its significant surface elevation: Mount Beerenberg, with peak elevation of approximately 2.3 km and mean diameter of approximately 15 km, dominates the island topography.[42,43]

Background buoyancy frequency and shear profiles gathered from radiosonde data were collected at 1200 UTC on 25

January 2000, a period when satellite imagery observed wavelike cloud banding downstream of the island.[11] These profiles are plotted in Fig. 4. Although both northward and eastward horizontal wind components were recorded, in the figure only the magnitude of the horizontal velocity is plotted. The direction of the flow was height dependent but deviated little from approximately 36° north of east throughout the domain, and so the flow was approximately two dimensional.

In an attempt to hindcast the observed wave patterns using a three-dimensional Fourier-ray model, Eckermann *et al.*[11] found that the waves were ducted, being trapped below an evanescent region near the top of the troposphere. Their results are reproduced in Fig. 5(a), which shows a vertical cross section of the vertical velocity field taken along a path aligned with the mean wind. This shows that a large amplitude wave with maximum vertical velocity ~ 4 m/s and with horizontal wavenumber $k \sim 0.14$ km^{-1} is ducted below an evanescent region approximately 10 km above the ground. Vertical velocities remain large and the waves propagate downstream as far as 200 km. Above the waveguide there is comparatively little downstream disturbance in the stratosphere.

Using a considerably more computationally expensive fully nonlinear numerical model, significantly different vertical velocity fields were predicted.[11] As shown in Fig. 5(b), the downstream vertical velocity does not remain large well beyond the generation point and there is significant wave energy in the stratosphere. Wave energy "trapped" in the waveguide escaped through the evanescent region upward in the vertical domain. The "leakiness" of the waveguide is due to tunneling of internal waves into the stratosphere, a phenomenon that the Fourier-ray model did not reproduce.

The Jan Mayen background profiles, plotted in Fig. 4, were input into the anelastic Taylor–Goldstein solver and the resulting transmission characteristics were found. The transmission coefficient is plotted in Fig. 6 for the entire range of incident extrinsic frequency ω and horizontal wavenumber k over which wavelike solutions exist at the bottom and top of the domain.

As in previous transmission coefficient plots, areas plotted in black correspond to regions in ω-k space for which transmission was not computed. In the areas on the far left

106601-7   Beyond ray tracing for internal waves. I

Phys. Fluids **20**, 106601 (2008)

(a) Fourier-Ray Solution
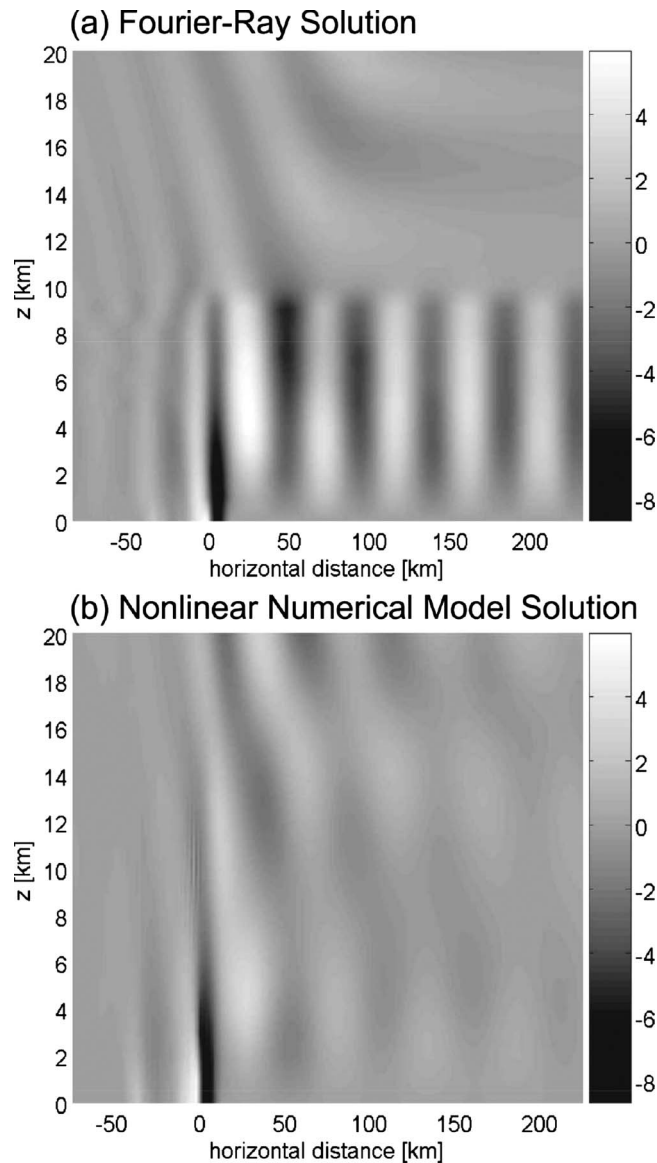

(b) Nonlinear Numerical Model Solution

FIG. 5. Vertical cross sections of vertical velocity in m s^{-1} (see grayscale bars) at $t=4$ h. (a) Fourier-ray solution. Minimum value is -7.8 m s^{-1} and maximum value is 6.1 m s^{-1}. (b) Nonlinear numerical model solution. Minimum value is -8.7 m s^{-1} and maximum value is 5.8 m s^{-1}. [Adapted from S. D. Eckermann, D. Broutman, J. Ma, and J. Lindeman, "Fourier-ray modeling of short-wavelength trapped lee waves observed in infrared satellite imagery near Jan Mayen," Mon. Weather Rev. **134**, 2830 (2006), with permission from the American Meteorological Society copyright agreement.]

and right sides of the plot, the extrinsic frequency and horizontal wavenumber were such that solutions were not wave-like at the top of the domain. The lower of the two dashed-dotted white lines is plotted where ω/k equals the minimum background horizontal flow speed; the upper white line is plotted where ω/k equals the maximum horizontal flow speed. In the region between these two extremes the incident wave speed matches the background flow speed somewhere in the vertical domain: The waves encounter a critical layer. Because the gradient Richardson number is larger than 1/4 everywhere in the flow, transmission across the critical layer was not computed.

In the region to the right of the dashed-dotted line in Fig.
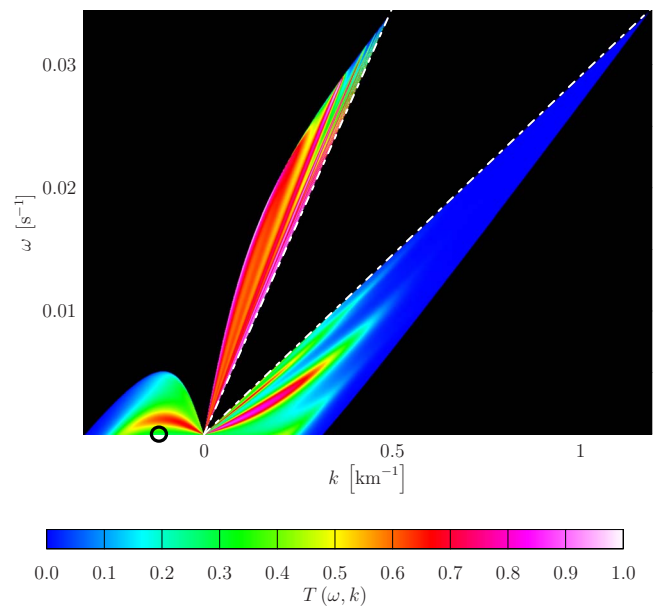

FIG. 6. (Color online) Transmission as a function of incident wave frequency and wavenumber for atmospheric conditions observed over Jan Mayen (as plotted in Fig. 4). The black circle about (k,ω) $=(-0.12$ km$^{-1},0)$ highlights the approximate frequency and horizontal wavenumber of the trapped waves shown in Fig. 5(a).

6, where waves move slower than the minimum horizontal flow in the background profiles, transmission is relatively weak.

For forward-propagating waves moving more quickly than the maximum horizontal flow speed, transmission is relatively high over nearly the entire region. Transmission decreases at larger frequencies but remains larger than 0.5 for nearly all wavenumbers in the region if $\omega < 0.02$ s^{-1}. There are bands in k-ω space with stronger transmission suggesting the waves are close to being resonantly ducted by the background state.[14] For negative horizontal wavenumbers (corresponding to upstream propagating waves relative to the surface wind), transmission is weak outside of a narrow band of relatively large transmission. Only relatively low frequency waves are possible in this regime.

Based on the nonlinear numerical simulation results shown in Fig. 5(b), the horizontal wavenumber of waves in the lee of Mount Beerenberg is estimated to be k $=-0.12$ km^{-1}. Being mountain waves, the extrinsic frequency is $\omega=0$. Using these values the transmission coefficient is found to be $\mathcal{T} \simeq 0.29$. This value is indicated by the circle on Fig. 6. Its calculation took 2 s on a 1.8 GHz PowerPC G5 CPU.

The corresponding magnitude and phase of the mass streamfunction are plotted in Fig. 7. The magnitude is plotted relative to the amplitude $|A^+|$ of the incident wave. Its value is larger than unity near the surface because ϕ is a superposition of the incident and reflected waves here.

The gray regions in Fig. 7 denote altitudes where the waves are evanescent. Thus we expect the phase lines to be vertically oriented in these regions and the waves should tilt into the wind otherwise. Indeed this behavior is observed in the nonlinear numerical model [Fig. 5(b)] although it is not
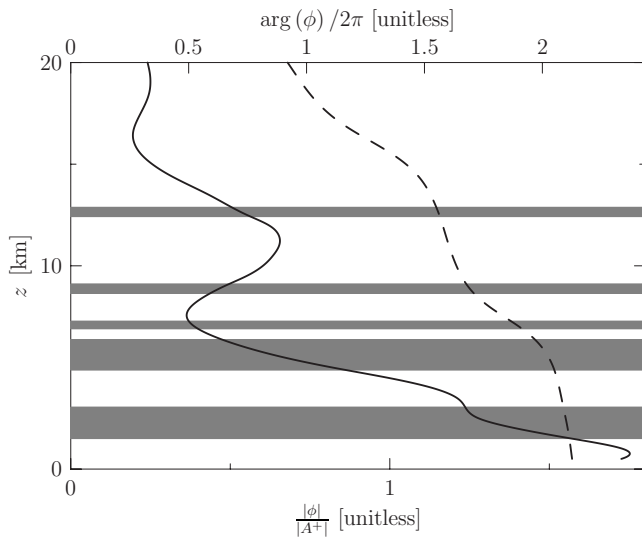
FIG. 7. Streamfunction magnitude (solid line) and phase (dashed line) calculated for waves with horizontal wavenumber $k = 0.14$ km^{-1} and frequency $\omega = 0.012$ s^{-1} using Jan Mayen background profiles presented in Fig. 4. Where the waves are evanescent are highlighted by the gray shaded regions.

captured by the Fourier-ray solution [Fig. 5(a)]. In these regions the streamfunction decreases rapidly. Beyond the evanescent region wavelike propagation is again possible and the streamfunction magnitude varies little. Thus, despite the presence of multiple evanescent levels in the troposphere and lower stratosphere, significant amounts of wave pseudoenergy can transmit into the middle atmosphere.

Using the computed transmission coefficient, an estimate for the rate at which energy escapes the duct is found. Perfectly trapped waves can be modeled as the superposition of incident and reflected waves. As such, the transmission coefficient is a measure of how much pseudoenergy $\mathcal{E}$ escapes the waveguide over each horizontal wavelength, $\lambda = 2\pi/k$,

$$\frac{1}{\mathcal{E}}\frac{\partial \mathcal{E}}{\partial x} = -\frac{\mathcal{T}}{\lambda}. \tag{19}$$

Thus the pseudoenergy remaining in the waveguide decays as

$$\mathcal{E}(x) \propto e^{-\mathcal{T}x/\lambda}. \tag{20}$$

Using the computed transmission coefficient, approximately 31% of the wave pseudoenergy will remain in the waveguide after propagating approximately four horizontal wavelengths. As the energy is related to the square of velocity, it is expected that vertical velocities near the ground four wavelengths downstream should be are approximately 56% of those at the beginning of the waveguide. These results are consistent with the nonlinear numerical results plotted in Fig. 5(b).

V. CONCLUSIONS

We developed a numerical method to predict the propagation of small-amplitude, two-dimensional anelastic internal gravity waves through nonrotating inviscid fluids. Compared with Boussinesq waves, anelastic effects act primarily to restrict the range of frequency and horizontal wavenumber

over which transmission is possible. As with the Boussinesq calculation, internal waves can tunnel across critical levels in a shear layer if the gradient Richardson number is less than 1/4 at that level.

Applied to background profiles observed over Jan Mayen Island, we found that waves could tunnel through an evanescent region near the tropopause and consequently radiate into the stratosphere. The corresponding estimate of the energy decay rate is consistent with satellite observations and fully nonlinear numerical simulations.[11] Fourier-ray tracing has the advantage of producing predictions of wave propagation in minutes rather than hours. Our calculation produces a better prediction of energy loss from waves in leaky duct and does so in seconds. The method has not been adapted for waves that encounter a stable critical because realistically nonlinear and viscous effects would play a role in this case. However, the method may usefully be adapted for use by general circulation models providing, in particular, a more reliable and computationally efficient means to estimate energy transmission through vertically localized evanescent regions in the middle atmosphere.

APPENDIX A: RELATION OF H_ρ TO N^2

Although the anelastic form of the Taylor–Goldstein equation involves both the density scale height H_ρ and the squared buoyancy frequency N^2, these quantities are not independent. Here we assume that $N^2(z)$ is specified and from this determine $H_\rho(z)$. The steps in this derivation are well established in the literature.

Using the definition in Eq. (10), the background potential temperature is given explicitly by

$$\bar{\theta} = \theta_0 \exp\left[\int_{z_0}^z \frac{1}{g}N^2(\tilde{z})d\tilde{z}\right]. \tag{A1}$$

The absolute pressure distribution is found by integrating the hydrostatic balance equation (4) and using Eq. (2),

$$\bar{p}(z) = p_{00}\left[1 - \frac{g}{c_p}\int_{z_0}^z \frac{d\tilde{z}}{\bar{\theta}(\tilde{z})}\right]^{1/\kappa}. \tag{A2}$$

Differentiating this equation and using background hydrostatic balance gives the expression for the background density,

$$\bar{\rho}(z) = \frac{p_{00}}{R\bar{\theta}(z)}\left[1 - \frac{g}{c_p}\int_{z_0}^z \frac{d\xi}{\bar{\theta}(\xi)}\right]^{(1-\kappa/\kappa)}. \tag{A3}$$

From this the density scale height can be found from the defining formula (11).

106601-9   Beyond ray tracing for internal waves. I

Phys. Fluids **20**, 106601 (2008)

APPENDIX B: FROBENIUS METHOD

The Taylor–Goldstein equation (8) is singular at critical layers, which occur at levels z where $\bar{\Omega}(z)=0$. The standard method used to integrate over such singularities is through the method of Frobenius.[39] This method is reviewed here as it is relevant to our study.

The Taylor–Goldstein equation is rewritten as

$$\bar{\Omega}^2\phi'' + \frac{\bar{\Omega}^2}{H_\rho}\phi' + \left(\frac{k\bar{U}'\bar{\Omega}}{H_\rho} - k^2\bar{\Omega}^2 + N^2k^2 + \bar{U}''k\bar{\Omega}\right)\phi = 0,$$
(B1)

and polynomial approximations are made to the coefficients near a singularity at z^*,

$$\bar{\Omega} = a\hat{z},$$
(B2a)

$$\frac{1}{H_\rho} = b(\hat{z}-z_1),$$
(B2b)

$$\frac{k\bar{U}'\bar{\Omega}}{H_\rho} - k^2\bar{\Omega}^2 + N^2k^2 + \bar{U}''k\bar{\Omega} = c(\hat{z}-z_2)(\hat{z}-z_3),$$
(B2c)

in which $\hat{z}=z-z^*$. Note, the third term of Eq. (B1) has been approximated by a quadratic rather than linear polynomial to account more accurately for the curvature of $\bar{U}$ near the singularity. The curvature of $\bar{\Omega}$ is neglected since this corresponds to the special case of a critical layer at the nose of a jet, a special case unlikely to be encountered often in realistic circumstances. It is unnecessary to include quadratic terms in Eqs. (B2a) and (B2b) because these only affect higher order terms in the Frobenius expansion.

To apply the method of Frobenius, ϕ is expanded as

$$\phi(z) = \hat{z}^r\sum_{n=0}^{\infty} f_n\hat{z}^n,$$
(B3)

where r and f_n remain to be found. The ϕ expansion is then substituted into Eq. (B1) and rearranged so that like powers of $\hat{z}$ are grouped together. The coefficients for each power of $\hat{z}$ must equal zero.

At leading order this restricts r to one of the following roots:

$$r = \frac{1}{2} \pm \sqrt{\frac{1}{4} - \frac{z_2z_3c}{a^2}}.$$
(B4)

If $0 < \mathrm{Ri}_g < 1/4$ at z^*, it turns out that Eq. (B4) requires r to have two distinct positive real values. A double root occurs if $\mathrm{Ri}_g=0$ (corresponding to $N^2=0$ at the critical level), in which case a logarithmic singularity occurs. If $\mathrm{Ri}_g > 1/4$ at z^*, r is complex valued. The imaginary part of r results in oscillations in ϕ whose wavelength becomes infinitesimally small as $\hat{z}\rightarrow 0$. In reality, such structure would then be influenced both by finite-amplitude and viscous effects. Because our model neglects such physics, we restrict ourselves here to circumstances in cases for which waves encounter a critical level with $\mathrm{Ri}_g < 1/4$.

At the next two higher orders, we find f_1 and f_2 in terms of f_0. Thus we construct an approximate solution for ϕ about the singularity which is matched to the integrated solution a small distance from the singularity.

In applying the Frobenius method, specific frequency and wavenumber combinations may result in numerical errors that prevent calculation of transmission coefficient. These errors are a consequence of the cutoff condition used to invoke the Frobenius solver. If the region over which the Frobenius solver is required is too large then the code may not be able to determine accurate polynomial fits for the anelastic Taylor–Goldstein equation, in which case transmission cannot be calculated. A filter is applied to suppress this spurious data. At points where the transmission coefficient cannot be computed, it is taken as the average of the immediately surrounding values.

[1] T. N. Palmer, G. J. Shutts, and R. Swinbank, "Alleviation of a systematic westerly bias in general circulation and numerical weather prediction models through an orographic gravity drag parametrization," Q. J. R. Meteorol. Soc. **112**, 1001 (1986).

[2] N. A. McFarlane, "The effect of orographically excited gravity wave drag on the general circulation of the lower stratosphere and troposphere," J. Atmos. Sci. **44**, 1775 (1987).

[3] R. S. Lindzen, "Turbulence and stress owing to gravity wave and tidal breakdown," J. Geophys. Res. **86**, 9707, DOI: 10.1029/JC086iC10p09707 (1981).

[4] D. Broutman, J. W. Rottman, and S. D. Eckermann, "Ray methods for internal waves in the atmosphere and ocean," Annu. Rev. Fluid Mech. **36**, 233 (2004).

[5] D. Broutman and J. W. Rottman, "A simplified Fourier method for computing the internal wavefield generated by an oscillating source in a horizontally moving, depth-dependent background," Phys. Fluids **16**, 3682 (2004).

[6] Y. Yamada, H. Fukunishi, T. Nakamura, and T. Tsuda, "Breaking of small-scale gravity waves and transition to turbulence observed in OH airglow," Geophys. Res. Lett. **28**, 2153, DOI: 10.1029/2000GL011945 (2001).

[7] M. J. Alexander, P. May, and J. Beres, "Gravity waves generated by convection in the Darwin area wave experiment," J. Geophys. Res. **109**, D20S04, DOI: 10.1029/2004JD004729 (2004).

[8] R. L. Walterscheid, G. Schubert, and D. G. Brinkman, "Small-scale gravity waves in the upper mesosphere and lower thermosphere generated by deep tropical convection," J. Geophys. Res. **106**, 31825, DOI: 10.1029/2000JD000131 (2001).

[9] J. B. Snively and V. P. Pasko, "Breaking of thunderstorm-generated gravity waves as a source of short-period ducted waves at mesopause altitudes," Geophys. Res. Lett. **30**, 2254, DOI: 10.1029/2003GL018436 (2003).

[10] S. D. Eckermann, A. Dornbrack, S. B. Vosper, H. Flentje, M. J. Mahoney, T. P. Bui, and K. S. Carslaw, "Mountain wave-induced polar stratospheric cloud forecasts for aircraft science flights during SOLVE/THESEO 2000," Weather Forecast. **21**, 42 (2006).

[11] S. D. Eckermann, D. Broutman, J. Ma, and J. Lindeman, "Fourier-ray modeling of short-wavelength trapped lee waves observed in infrared satellite imagery near Jan Mayen," Mon. Weather Rev. **134**, 2830 (2006).

[12] C. Eckart, "Internal waves in the ocean," Phys. Fluids **4**, 791 (1961).

[13] D. C. Fritts and L. Yuan, "An analysis of gravity wave ducting in the atmosphere: Eckart's resonances in thermal and Doppler ducts," J. Geophys. Res. **94**, 18455, DOI: 10.1029/JD094iD15p18455 (1989).

[14] B. R. Sutherland and K. Yewchuk, "Internal wave tunnelling," J. Fluid Mech. **511**, 125 (2004).

[15] R. S. Lindzen and K.-K. Tung, "Banded convective activity and ducted gravity waves," Mon. Weather Rev. **104**, 1602 (1976).

[16] R. S. Lindzen and J. W. Barker, "Instability and wave over-reflection in stably stratified shear flow," J. Fluid Mech. **151**, 189 (1985).

[17] I. A. Eltayeb and J. F. McKenzie, "Critical-level behaviour and wave amplification of a gravity wave incident upon a shear layer," J. Fluid Mech. **72**, 661 (1975).

[18] C. A. Van Duin and H. Kelder, "Reflection properties of internal gravity

waves incident upon a hyperbolic tangent shear layer," J. Fluid Mech. **120**, 505 (1982).

[19]T.-A. Wang and Y.-L. Lin, "Wave ducting in a stratified shear flow over a two-dimensional mountain. Part 1: General linear criteria," J. Atmos. Sci. **56**, 412 (1999).

[20]G. L. Brown and B. R. Sutherland, "Internal wave tunnelling through non-uniformly stratified shear flow," Atmos.-Ocean. **45**, 47 (2007).

[21]J. T. Nault and B. R. Sutherland, "Internal wave tunnelling across a mixed region," Phys. Fluids **19**, 016601 (2007).

[22]P. G. Drazin and W. H. Reid, *Hydrodynamic Stability* (Cambridge University Press, Cambridge, 1981).

[23]T. Beer, *Atmospheric Waves* (Wiley, New York, 1974).

[24]E. E. Gossard and W. H. Hooke, *Waves in the Atmosphere* (Elsevier, Amsterdam, 1975).

[25]R. B. Smith, "Hydrostatic airflow over mountains," in *Advances in Geophysics*, edited by B. Saltzman (Academic, New York, 1989), Vol. 31, pp. 1–41.

[26]S. D. Mobbs and M. S. Darby, "General method for the linear stability analysis of stratified shear flows," Q. J. R. Meteorol. Soc. **115**, 915 (1989).

[27]G. J. Shutts, "Gravity-wave drag parametrization over complex terrain: the effect of critical level absorption in directional wind shear," Q. J. R. Meteorol. Soc. **121**, 1005 (1995).

[28]T. A. Shaw and T. G. Shepherd, "Wave-activity conservation laws for the three-dimensional anelastic and Boussinesq equations with a horizontally homogeneous background flow," J. Fluid Mech. **594**, 493 (2008).

[29]G. L. Brown, A. B. G. Bush, and B. R. Sutherland, "Beyond ray tracing for internal waves. II. Finite-amplitude effects," Phys. Fluids **20**, 106602 (2008).

[30]R. Wilhelmson and Y. Ogura, "Pressure perturbation and numerical modeling of a cloud," J. Atmos. Sci. **29**, 1295 (1972).

[31]F. B. Lipps and R. S. Hemler, "A scale analysis of deep moist convection and some related numerical calculations," J. Atmos. Sci. **39**, 2192 (1982).

[32]Y. Ogura and N. A. Phillips, "Scale analysis of deep and shallow convection in the atmosphere," J. Atmos. Sci. **19**, 173 (1962).

[33]G. K. Batchelor, "The conditions for dynamical similarity of motions of a frictionless perfect-gas atmosphere," Q. J. R. Meteorol. Soc. **79**, 224 (1953).

[34]J. F. Scinocca and T. G. Shepherd, "Nonlinear wave-activity conservation laws and Hamiltonian structure for the two-dimensional anelastic equations," J. Atmos. Sci. **49**, 5 (1992).

[35]R. S. Scorer, "Theory of waves in the lee of mountains," Q. J. R. Meteorol. Soc. **75**, 41 (1949).

[36]M. G. Wurtele, R. D. Sharman, and T. L. Keller, "Analysis and simulations of a troposphere-stratosphere gravity wave model. Part I," J. Atmos. Sci. **44**, 3269 (1987).

[37]T. L. Keller, "Implications of the hydrostatic assumption on atmospheric gravity waves," J. Atmos. Sci. **51**, 1915 (1994).

[38]W. H. Press, B. P. Flannery, S. A. Teukolsky, and W. T. Vetterling, *Numerical Recipes: The Art of Scientific Computing*, 2nd ed. (Cambridge University Press, New York, 1993).

[39]J. R. Booker and F. P. Bretherton, "The critical layer for internal gravity waves in shear flow," J. Fluid Mech. **27**, 513 (1967).

[40]S. A. Maslowe, "Weakly nonlinear stability theory of stratified shear flows," Q. J. R. Meteorol. Soc. **103**, 769 (1977).

[41]S. A. Maslowe, "Critical layers in shear flows," Annu. Rev. Fluid Mech. **18**, 405 (1986).

[42]B. Gjevik and T. Marthinsen, "3-dimensional lee-wave pattern," Q. J. R. Meteorol. Soc. **104**, 947 (1978).

[43]A. Simard and W. R. Peltier, "Ship waves in the lee of isolated topography," J. Atmos. Sci. **39**, 587 (1982).